Modeling, Design, Fabrication, and Testing of InP Gunn Devices in the D-band (110 GHz - 170 GHz) [1]

R. Kamoua [2], H. Eisele, J. R. East, G. I. Haddad,
G. Munns, and M. Sherwin

Solid-State Electronics Laboratory
Department of Electrical Engineering and Computer Science
The University of Michigan, Ann Arbor, MI 48109-2122

Abstract

The development of fundamental Gunn sources for D-band frequencies requires improvements of doping profiles, processing technology, and circuit design. We have developed a technology for fabricating InP Gunn diodes using an InGaAs etch-stop layer between the InP substrate and the device layers. The epitaxial layers were grown by CBE. During device processing, the substrate is completely removed. Substrateless devices with an n^+ InGaAs cap layer are expected to have reduced contact and series resistances, and skin effect losses. This technology gives better uniformity and control of the device geometry across the processed chip.

InP Gunn devices with a 1.7 μm long active region (doping : 9×10^{15} cm^{-3}) have been mounted on copper heat sinks. Two tapered leads were then bonded to the diode and to four quartz standoffs. As a preliminary result, an output power of 13 mW at 82 GHz was obtained. Based on these RF measurements, we determine appropriate material parameters to be used in the Ensemble Monte Carlo model. Subsequently, we use this model to design and evaluate the performance of InP Gunn Devices for D-band frequencies. Using the same technology, we are currently processing Gunn devices with a 1μm long active region for operation at higher frequencies.

[1]This work was supported by the Center for Space Terahertz Technology under Contract No. NAGW-1334

[2]R. Kamoua is currently with the Department of Electrical Engineering, State University of New York at Stony Brook, Stony Brook, NY 11794-2350

1 Introduction

Gunn devices are widely used as local pump oscillators in the W-band frequency region. At these frequencies, the technology is well developed. In particular at 94 GHz, GaAs and InP Gunn devices are available with very good performance. At frequencies above 100 GHz, the situation is quite different. Although there is a strong demand for sources at these frequencies, fundamental Gunn devices are generally not available. There are two reasons. First, most of the research effort has been focused at 94 GHz. Second, extending the fundamental oscillation frequency of Gunn devices into the submillimeter region is exceedingly difficult because the Gunn effect is being pushed to its high frequency limit.

This paper discusses a systematic approach toward the *modeling, design, fabrication*, and *testing* of InP Gunn devices in the D-band region. Compared with GaAs, InP material parameters are more favorable for operating Gunn devices in the D-band. The approach taken in this work is both experimental and theoretical. Experimentally, the conventional processing technology is improved by incorporating etch-stop layers in the wafer design. The RF results obtained from devices fabricated using this technology are then used to improve the accuracy of the theoretical model. Subsequently, the improved model is used to design the optimum Gunn structure for the desired frequency of operation.

2 Simulation Model

The self consistent Ensemble Monte Carlo model is used to estimate the performance of InP Gunn devices at high frequencies. This model is an extension of the one particle Monte Carlo technique [1]. In order to describe the transport process in a structure with nonuniform doping and with time varying fields, an ensemble of electrons needs to be simulated simultaneously. The electric field has to be updated regularly since it is evolving as the electrons redistribute in the structure. The analysis is carried out assuming the device behavior is mainly one dimensional which is justified for two terminal devices. A diode structure of length L is divided into cells of equal length (Δx = 50 Å). Any attributes of the electrons are averaged over each cell and assigned to the midway position of the cell. The cell size should be smaller than the smallest Debye length in the structure which occurs at the highly doped regions.

The simulation algorithm consists of monitoring the evolution in real space and momentum space of an ensemble of electrons. The simulation time is partitioned into time steps ($\Delta t = 5\times10^{-15}$ sec) each terminated by a call to a Poisson solver in order to update the field. In each time step every electron is submitted to successive free flights terminated by a scattering process which is selected using a random number generator. Electrons crossing cell boundaries are temporarily stopped at that boundary and then resumed with the electric field in the new cell. An analogous procedure is followed when it is time to update the electric field and the electron is in the middle of a free flight. In this case the remaining flight time is stored, and the flight is resumed when all other electrons are simulated for one time step, the carrier density is calculated, and the electric field is updated. The predicted performance of a particular Gunn structure is estimated by applying an RF voltage across the device and simulating the current response over many RF periods (about 10). The resulting particle current density is Fourier analyzed and the fundamental component is

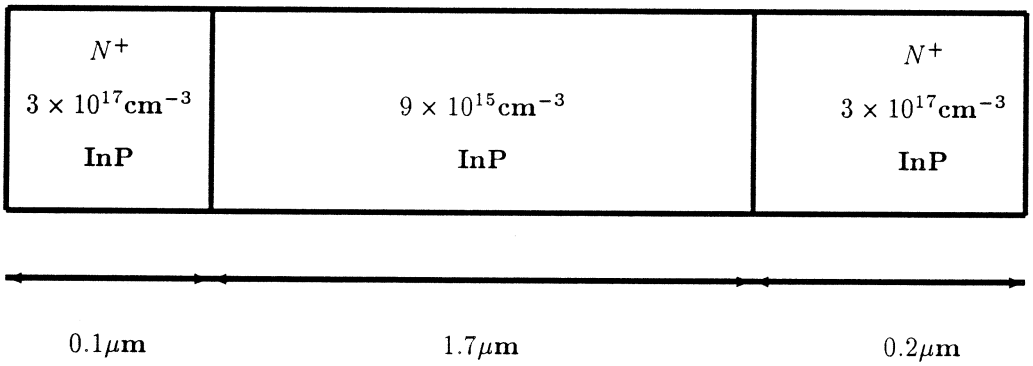

Figure 1: Dimensions and doping profile of Gunn structures.

used to determine the device admittance. The RF output power is estimated by considering the Gunn device in a resonant circuit represented by a load resistance and a resonating inductance. A series resistance is included in the equivalent circuit that takes into account effects of contact resistances, any substrate resistances, and skin effect losses.

The accuracy of the Monte Carlo model is strongly dependent on the accuracy of the material parameters used. Unfortunately, one finds a wide range of values that are being used in the literature. In particular, some of the material parameters that are important to the Gunn effect have the following range of values ([2, 3, 4, 5]):

$\Gamma - L$ valley separation (eV)	0.4	$\Longleftrightarrow$	0.832,
L valley effective mass ratio ($\frac{m}{m_0}$)	0.26	$\Longleftrightarrow$	0.4,
$\Gamma - L$ coupling constant ($\times 10^9$ eV.cm^{-1})	0.1	$\Longleftrightarrow$	2.5,
$\Gamma - X$ coupling constant ($\times 10^9$ eV.cm^{-1})	0.43	$\Longleftrightarrow$	1.0.

There is more than an order of magnitude uncertainty in the Γ to L intervally coupling constant. In the next section, the material parameters that yield the best agreement with the RF measured results will be identified.

3 Method for Extracting Accurate InP Material Parameters for a 3-Valley Nonparabolic EMC Model

The appropriate material parameters are determined by comparing measurements at high frequencies with results predicted by the model. The structure considered for comparison is shown in Figure 1. It has 1.7 μm long active region doped at 9×10^{15} cm^{-3}, a 0.1μm cathode region doped at 3×10^{17} cm^{-3} and a 0.2 μm anode region doped at 3×10^{17} cm^{-3}.

An InP wafer with this structure has been processed. The relevant fabrication technology will be described later. Diodes with various sizes have been mounted on copper heat sinks. Tapered ribbons were then used to bond a diode to four quartz standoffs. A 40 μm diode was tested in a W-band resonant cavity with the following results:

Bias voltage	4.0 V to 4.5 V,
Oscillation frequency	82 GHz,
output power	13 mW,
conversion efficiency	1 %,
DC current	350 mA.

The structure shown in Figure 1 is simulated using the model described above. The DC bias is 4.5 V, the RF voltage is 1.0 V, and the operating temperature is assumed to be 400 K. The material parameters are considered to be accurate if oscillations at 82 GHz are predicted with a performance comparable to experimental results. The starting combination of parameters is listed in Table 1 and is referred to as the *initial parameter set.* No oscillations occurred with this set of values for frequencies ranging from 75 GHz to 120 GHz. It appears that the $\Gamma - L$ intervalley energy separation of 0.832 eV is too large. As a result, the following modifications to the initial set are considered:

- Case 1. The same parameters as the initial set are used except $\Gamma - L$ valley separation = 0.6 eV. No oscillations occurred at 82 GHz.
- Case 2. The same parameters as the initial set are used except $\Gamma - L$ valley separation = 0.4 eV. No oscillations occurred at 82 GHz.
- Case 3. The same parameters as the initial set are used except $\Gamma - L$ energy separation = 0.4 eV and $\Gamma - X$ energy separation = 0.7 eV. No oscillations occurred at 82 GHz.
- Case 4. The same parameters as the initial set are used except L valley effective mass ratio = 0.4 and X valley effective mass ratio = 0.4. No oscillations occurred at 82 GHz.
- Case 5. The same parameters as the initial set are used except $\Gamma - L$ coupling constant = 1.0×10^9 eV.cm^{-1}. No oscillations occurred at 82 GHz.
- Case 6. The same material parameters as the initial set are used except $\Gamma - L$ energy separation = 0.5 eV, $\Gamma - X$ energy separation = 0.8 eV, $\Gamma - L$ coupling constant = 1.0×10^9 eV.cm^{-1} and $\Gamma - X$ coupling constant = 1.0×10^9 eV.cm^{-1}. Very weak oscillations were obtained. The efficiency was 0.032 % and the output power was 0.22 mW.
- Case 7. The same parameters as the initial set are used except $\Gamma - L$ energy separation = 0.45 eV, $\Gamma - X$ energy separation = 0.775 eV, L valley effective mass ratio = 0.4 eV, X valley effective mass ratio = 0.4 eV, $\Gamma - L$ coupling constant = 1.0×10^9 eV.cm^{-1}, $\Gamma - X$ coupling constant = 1.0×10^9 eV.cm^{-1} and acoustic deformation potential = 5 eV. Oscillations were obtained at 82 GHz even though the DC bias was 4.0 V instead of 4.5 V. With 1.0 V RF voltage, the predicted output power for a 40 μm diode was 7.2 mW with 0.52 % efficiency.

The last parameter set appears to be promising and was considered in more detail. At an RF voltage of 1.5 V, the predicted efficiency was 1.1 % and the predicted output power

Energy Separation (eV)	Γ-L	0.832
	Γ-X	1.5
Effective Mass ($\frac{m^*}{m_0}$)	Γ	0.082
	L	0.26
	X	0.325
Nonparabolicity factor ($[eV]^{-1}$)	Γ	0.83
	L	0.23
	X	0.38
Intervalley Coupling Constant (10^9 eV.cm^{-1})	Γ-L	0.506
	Γ-X	0.498
	L-X	0.468
	L-L	0.575
	X-X	0.28
Acoustic Deformation Potential (eV)	Γ	7
	L	7
	X	7
LO Phonon Energy (eV)	Γ	0.043
	L	0.0423
	X	0.0416
Static Dielectric Constant		12.61
Optical Dielectric Constant		9.61

Table 1: InP initial material parameter set.

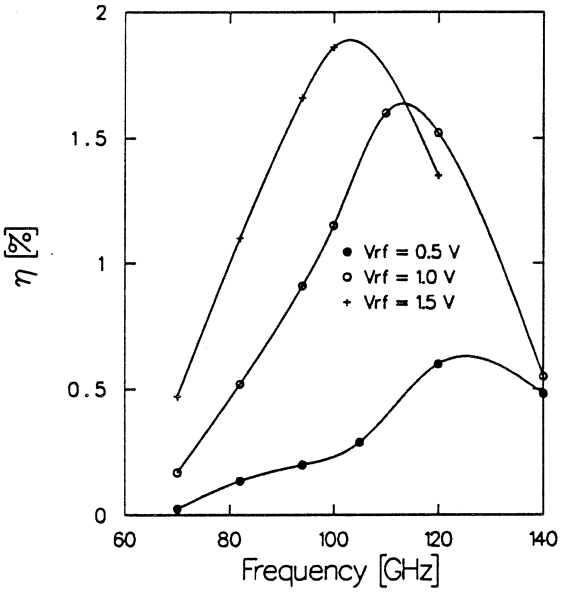

Figure 2: Efficiency vs. frequency for a 1.7 μm long InP Gunn device doped at 9×10^{15} cm^{-3}. Diameter = 40 μm, Vdc = 4.0 V, T = 450 K.

was 14.9 mW for a 40 μm diode. The necessary load resistance for matching the diode was 6.5 Ω. The simulated DC current density has a value of 2.7×10^4 $A.cm^{-2}$ which results in a current of 340 mA. The simulated device performance is in good agreement with the measured RF results. In summary, we found it necessary to decrease the intervalley energy separation and increase the electron effective mass in the upper valleys and the intervalley deformation potentials in order to obtain oscillations at 82 GHz. The actual device was operated at higher temperature than room temperature. This suggests that the lower values for the intervalley separation and the higher values for the deformation potentials might be caused by temperature effects on the band-structure. The last parameter set will be used to analyze various InP Gunn structures. In the next section, the 1.7 μm structure will be considered in more detail.

4 Simulation of 1.7 μm InP Gunn Devices

The results presented in this section correspond to a DC bias voltage of 4.0 V and an operating temperature of 450 K. For comparison purposes, the load resistance was adjusted so that the device area is 40 μm. Figure 2 shows a comparison of the conversion efficiency as a function of frequency for three RF voltage amplitudes: 0.5 V, 1.0 V and 1.5 V. The peak efficiency for a 1.5 V RF voltage is 1.86 % at 100 GHz. The corresponding comparison of the output power is shown in Figure 3. A peak power of 23 mW at 100 GHz was obtained for the case where the RF voltage is 1.5 V.

In general, the operating temperature is 80 K to 90 K above the room temperature. Therefore, it is possible to extract more power by either increasing the device area or the DC bias or a combination of both. Increasing the device area is limited by thermal effects

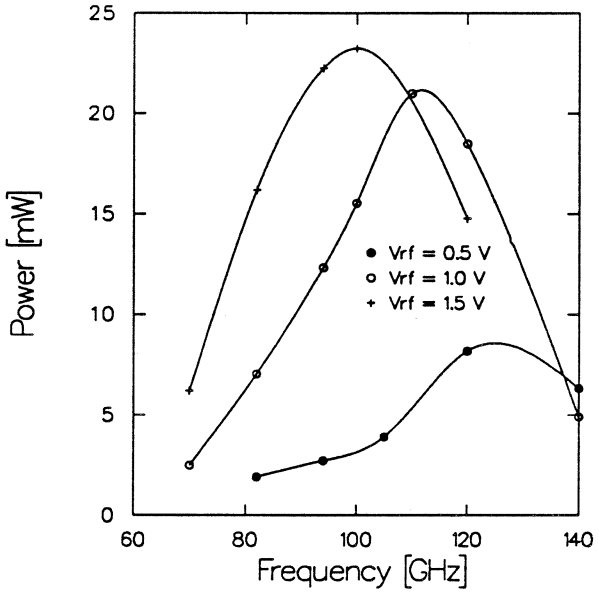

Figure 3: Power vs. frequency for a 1.7 μm long InP Gunn device doped at 9×10^{15} cm^{-3}. Diameter = 40 μm, Vdc = 4.0 V, T = 450 K.

and by the minimum load provided by the resonant circuit. On the other hand, increasing the DC bias voltage is limited by thermal effects and breakdown due to the large electric field at the anode. For example, increasing the diode diameter from 40 μm to 60 μm results in 50 mW output power at 100 GHz with an RF voltage of 1.5 V. The required matching load is 2 Ω compared to 3.75 Ω for the smaller device and the temperature increase is 120 K compared to 86 K.

5 Simulation of 1.0 μm InP Gunn Devices for Operation in D-band Frequency Region

The 1.7 μm device considered in the previous section had an optimum operating frequency around 100 GHz. For higher frequencies in D-band, structures with shorter active regions need to be considered. In this section, simulation results of a 1 μm long InP device are presented.

5.1 Flat Doping Profile

Two flat doping profiles in the active region 1×10^{16} cm^{-3} and 2×10^{16} cm^{-3} are considered. Figure 4 compares the corresponding efficiency as a function of frequency for a DC bias of 4.0 V, an RF voltage of 0.5 V, and an operating temperature of 450 K. The structure with 2×10^{16} cm^{-3} doping results in a higher efficiency at all frequencies. The output power into a 2 Ω load is shown in figure 5. Near 160 GHz, the predicted output power from the highly doped structure is more than 5 times higher than the output power from the low doped structure. However, for a meaningful comparison, thermal effects and current density levels

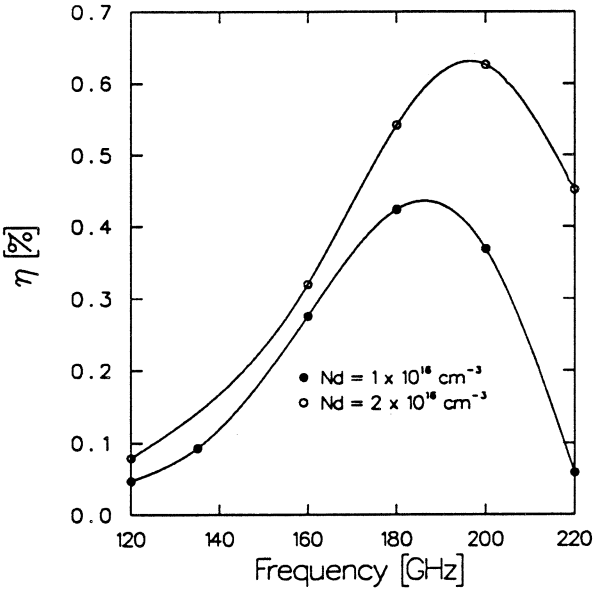

Figure 4: Efficiency versus frequency for a 1.0 μm long InP Gunn device. Vdc = 4.5 V, Vrf = 0.5 V, R_L = 2 Ω, T = 450 K.

need to be considered.

The DC current density in the structure with a lower doping is about 3.95×10^4 A.cm^{-2} at 160 GHz whereas it is about 6.7×10^4 A.cm^{-2} for the other structure. The device with the higher doping has a very large current density which results in an operating temperature approaching the limit for a 30 μm diameter device. For smaller diodes, bonding becomes very difficult. Therefore, there is a need for improving the efficiency while keeping the current density from increasing rapidly. It will be shown in the next section that a graded doping profile in the active region provides such an improvement.

5.2 Graded Doping Profile

This section examines methods of improving the efficiency of InP Gunn devices and optimizing the design for operation around 160 GHz. In addition to the structure with a flat doping of 1×10^{16} cm^{-3}, three linearly graded doping profiles are considered:

	N_1 ($\times10^{16}$ cm^{-3})	N_2 ($\times10^{16}$ cm^{-3})
Structure 1	1.0	1.0
Structure 2	0.8	1.5
Structure 3	0.8	3.0
Structure 4	0.8	4.0

In the above table, N_1 is the doping density in the active region at the cathode side and N_2 is the corresponding doping at the anode side. The results presented in this section correspond to a bias of 4.0 V, an RF voltage of 1.0 V, an operating temperature of 450 K,

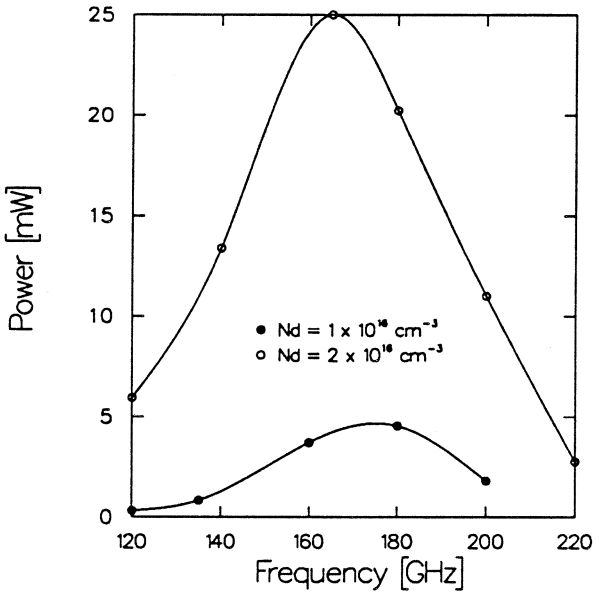

Figure 5: Power versus frequency for a 1.0 μm long InP Gunn device. Vdc = 4.5 V, Vrf = 0.5 V, R_L = 2 Ω, T = 450 K.

and a matching load of 2 Ω.

Figure 6 shows the efficiency versus frequency for the three structures. The efficiency is increasing as the doping profile becomes steeper. At 180 GHz, structure 3 results in 2 % efficiency which is twice the efficiency obtained from structure 1. A comparison of the output power is shown in Figure 7. The optimum frequency for power generation is 160 GHz where structure 3 resulted in 73.4 mW compared with 8.6 mW for structure 1. The DC current density in structure 3 is 5.18×10^4 A.cm^{-2} compared with 3.84×10^4 A.cm^{-2} in structure 1 at 160 GHz. This increase in the current density is much smaller than the corresponding increase in the 2×10^{16} cm^{-3} doped structure. Structure 4 has higher efficiencies than structure 3 but the current is also higher. For diodes with a mesa diameter of 30 μm or larger, structure 3 is likely to be the optimum design for operation at 160 GHz.

The graded doping profile results in a higher electric field near the cathode and a lower field near the anode due to electron diffusion toward the lower doped region. This change in the field has two consequences: first, a higher cathode field results in a larger fraction of the electrons transferring to the upper valleys, second, a lower anode field permits application of a larger DC bias without breakdown. The electric field in structure 1 peaks at 125 kV.cm^{-1} near the anode side whereas the field in structure 4 is less than 100 kV.cm^{-1} at the anode.

In addition to improving the efficiency and reducing the field at the anode, a graded doping profile provides a modest increase in the current density. The graded doping profile can provide the same performance as the flat doped profile with a smaller current density. The reason is that the higher fraction of the electron population transferring to the upper valleys in the graded structure results in a reduction of the average velocity. This is not the case for the structure with a flat doping where an increase in the carrier density does not alter the distribution of the field across the structure. Figure 8 compares the current

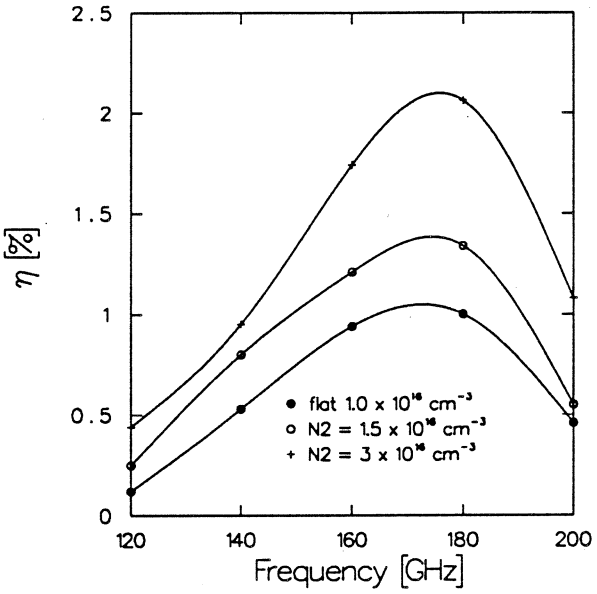

Figure 6: Efficiency versus frequency for a 1.0 μm InP Gunn device. Vdc = 4.0 V, Vrf = 1.0 V, RL = 2 Ω, T = 450 K.

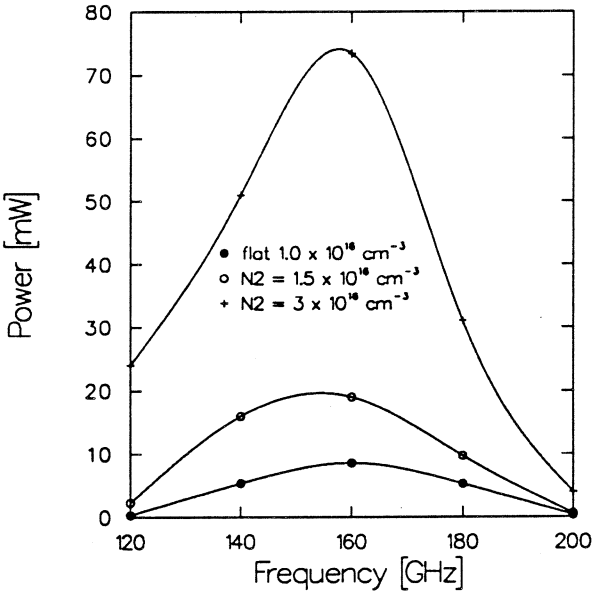

Figure 7: Power versus frequency for a 1.0 μm InP Gunn device. Vdc = 4.0 V, Vrf = 1.0 V, RL = 2 Ω, T = 450 K.

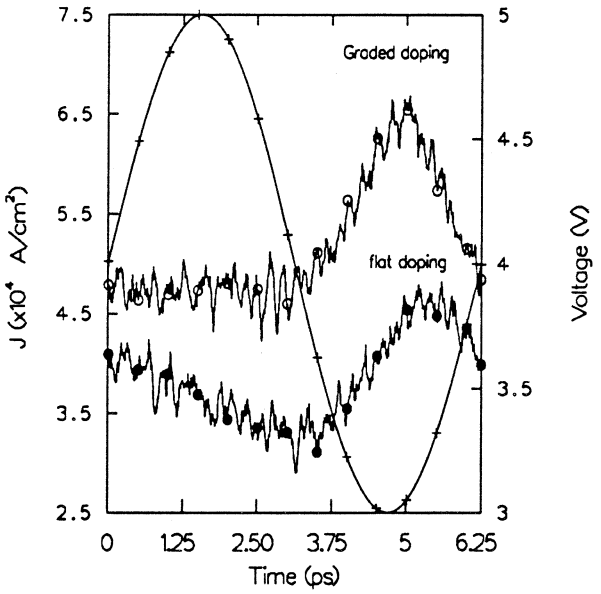

Figure 8: Comparison of the current density in structure 1 and structure 3 at 160 GHz. Vdc = 4.0 V, Vrf = 1.0 V, T = 450 K.

waveforms in one RF period as obtained from structure 1 and structure 3. The current density in structure 3 resembles a pulse 180 degrees out of phase with the RF voltage whereas in structure 1, it is more sinusoidal and is not perfectly out of phase. This shows that structure 3 is more efficient and the space charge layers are more developed.

To verify that the highly doped side of the active region should be at the anode side for best performance, structure 3 was considered with the opposite polarity. Figure 9 shows a comparison of the output power as a function of frequency. The structure with the doping decreasing toward the anode contribute to much smaller output power levels when compared with structure 3. An examination of the electric field revealed a peak electric field near the anode close to 200 $kV.cm^{-1}$ compared with 100 $kV.cm^{-1}$ in structure 3. In addition the current density is higher, at 160 GHz it has a average value of 6.9×10^4 $A.cm^{-2}$ compared with 5.2×10^4 $A.cm^{-2}$ in structure 3.

6 InP GUNN DEVICE TECHNOLOGY

Among the many techniques used for fabricating Gunn devices, the most common are based on the Integral Heat Sink process (IHS) [7, 8] or the flip-chip process [9]. In the IHS process, the heat sink is formed as an integral part of the diode. The wafer front side is metallized and plated with copper, silver, or gold to a thickness of several thousands of an inch. The substrate is chemically or mechanically thinned to a thickness of 10 μm to 15 μm . Next, ohmic contacts are metallized and standard photoresist techniques are used to define the mesas. Individual chips are then mounted in standard packages. In the flip-chip process the mesas are defined on the epitaxial side. The mesa chip is then flipped and mounted on a heat sink pedestal. Finally, the substrate is thinned to about 100 μm .

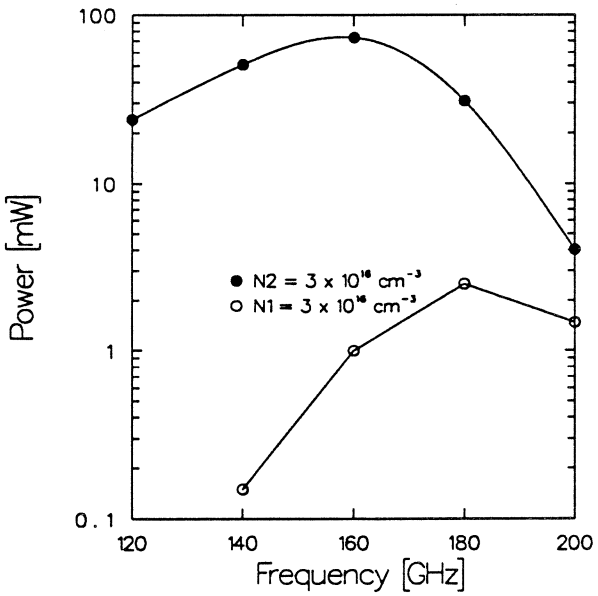

Figure 9: Comparison of the power versus frequency for structure 3 with different bias polarities . Vdc = 4.0 V, Vrf = 1.0 V, RL = 2 Ω, T = 450 K.

These two processing techniques have been used successfully for fabricating Gunn devices in the W-band. At higher frequencies, it is necessary to reduce further the substrate thickness to minimize the series resistance. In addition, the smaller size of the mesas presents new challenges to the bonding procedure. In this chapter a new fabrication technology allowing the complete removal of the substrate is developed. This process is an extension of the integral heat sink technique with the additional step of plating the top contact to facilitate bonding.

Figure 10 shows the epitaxial layers of an unprocessed InP wafer. The different layers, starting from the n^+ doped substrate consist of

- an n^+ InP substrate,
- a 0.5 μm n^+ InGaAs layer doped at 2.0×10^{18} cm^{-3},
- a 0.6 μm n^+ InP contact layer doped at 2.0×10^{18} cm^{-3},
- a 1.0 μm n InP active region doped doped at 1.0×10^{16} cm^{-3},
- a 0.2 μm n^+ InP contact layer doped at 2.0×10^{18} cm^{-3}, and
- a 0.1 μm n^+ InGaAs cap layer doped at 2.0×10^{18} cm^{-3}.

Prior to processing the wafer, the doping profile in the active region is characterized through C-V measurements. To perform these measurements, the top n^+ InGaAs and InP layers are chemically etched from a small sample so that Schottky contacts can be formed. The processing sequence for Gunn device fabrication is shown in figure 11 and described below.

6.1 Island Definition and Integral Heat Sink Formation

The first step consists of defining square islands approximately 400 μm $\times$ 400 μm in size separated on all sides by 100 μm wide trenches. These trenches are etched down to the InGaAs etch-stop layer. An n-ohmic contact (Ni/Ge/Au/Ti/Au) is evaporated over the whole surface and then gold is plated to a thickness of 25 μm to form the integral heat sink. The top InGaAs cap layer reduces the contact resistance [10] of the ohmic contact because InGaAs has a lower bandgap than GaAs. The isolation provided by the trenches is helpful in reducing the cracking of the semiconductor epilayers during the annealing process. Cracks occur because the gold heat sink and the InP semiconductor have different thermal expansion coefficients. Figure 11(a) shows a cross section of the sample at the end of the gold plating.

6.2 Substrate Thinning and Top Contact Definition

The InGaAs layer, referred to as an etch-stop layer, permits the complete removal of the substrate by chemical etching. The chemical solution HCl:H_2O (4:1) selectively etches InP and does not etch InGaAs. Once the substrate is removed, the InGaAs etch-stop layer is etched away using H_3PO_4:H_2O_2:H_2O (1:1:8) which does not attack the InP n^+ region. Standard lift-off techniques are used to define circular diodes with sizes varying from 30 to 65 μm in diameter which are then metallized to form n-ohmic contacts. Figure 11(b) shows a cross section of the sample after the substrate thinning and the heat sink formation.

6.3 Gold Plating of Top Contacts

In the standard IHS technique, the next step would be to etch the mesa. However problems in bonding have been encountered due to the thin ohmic contact. A thick ohmic contact is obtained by plating gold on top of the evaporated ohmic contacts. A conductive metal layer is needed to electroplate uniformly over all the contacts. A Ti/Au/Ti layer is evaporated over the whole surface, then an alignment over the ohmic contacts is used to open holes in a thick photoresist (3 μm). The photoresist is removed from a small region at the edge of the sample. The exposed Ti layer is also removed in Buffered HF and the sample is plated for a thickness of 2 μm - 3 μm. Figure 11(c) shows a cross section of the sample after the plating step.

6.4 Mesa Definition and Annealing

The final step before mounting individual chips consists of etching the mesas and annealing the ohmic contacts. The final structure is shown in figure 11(d).

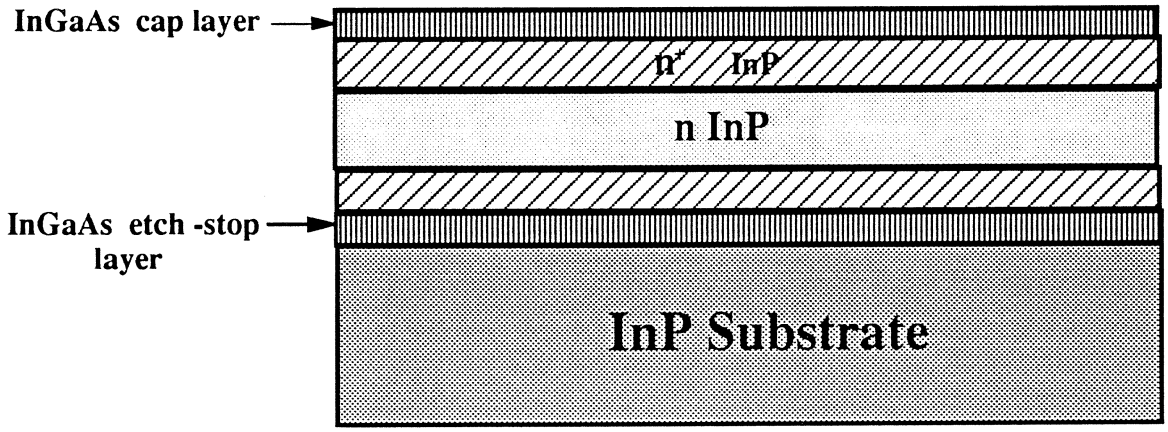

Figure 10: InP Gunn structure

7 Conclusions

A new method has been developed for estimating the material parameters used in the Monte Carlo model. By comparing simulation and experimental results in the W-band, we obtained more accurate material parameters. *Lower* values for the intervalley energy separation and *higher* values for the deformation potentials than stated in the literature were used. A possible explanation for these trends is the high operating temperature of the Gunn device which perturbs the band-structure.

Using these parameters, it was shown that it is possible to operate fundamental mode InP Gunn devices in the D-band. The performance of a flat doped structure can be considerably improved by employing a graded doping profile in the active region. Specifically, a linearly graded doping increasing from the cathode toward the anode improves the conversion efficiency, the output power, reduces the electric field at the anode, and results in a smaller current density compared with a flat profile. A structure with a doping decreasing toward the anode is not desirable because it increases the electric field at the anode and does not reduce the dead zone. As a result, the device breaks down at lower voltages and the performance is degraded.

A processing technology for GaAs and InP Gunn devices has been developed based on the integral heat sink processing technique. An Etch-stop layer between the substrate and the epilayers was included in the wafer design in order to completely remove the substrate and obtain better uniformity across the chip. InGaAs cap layers were used to reduce the contact resistance. A process was developed for plating the top contacts with gold to facilitate bonding.

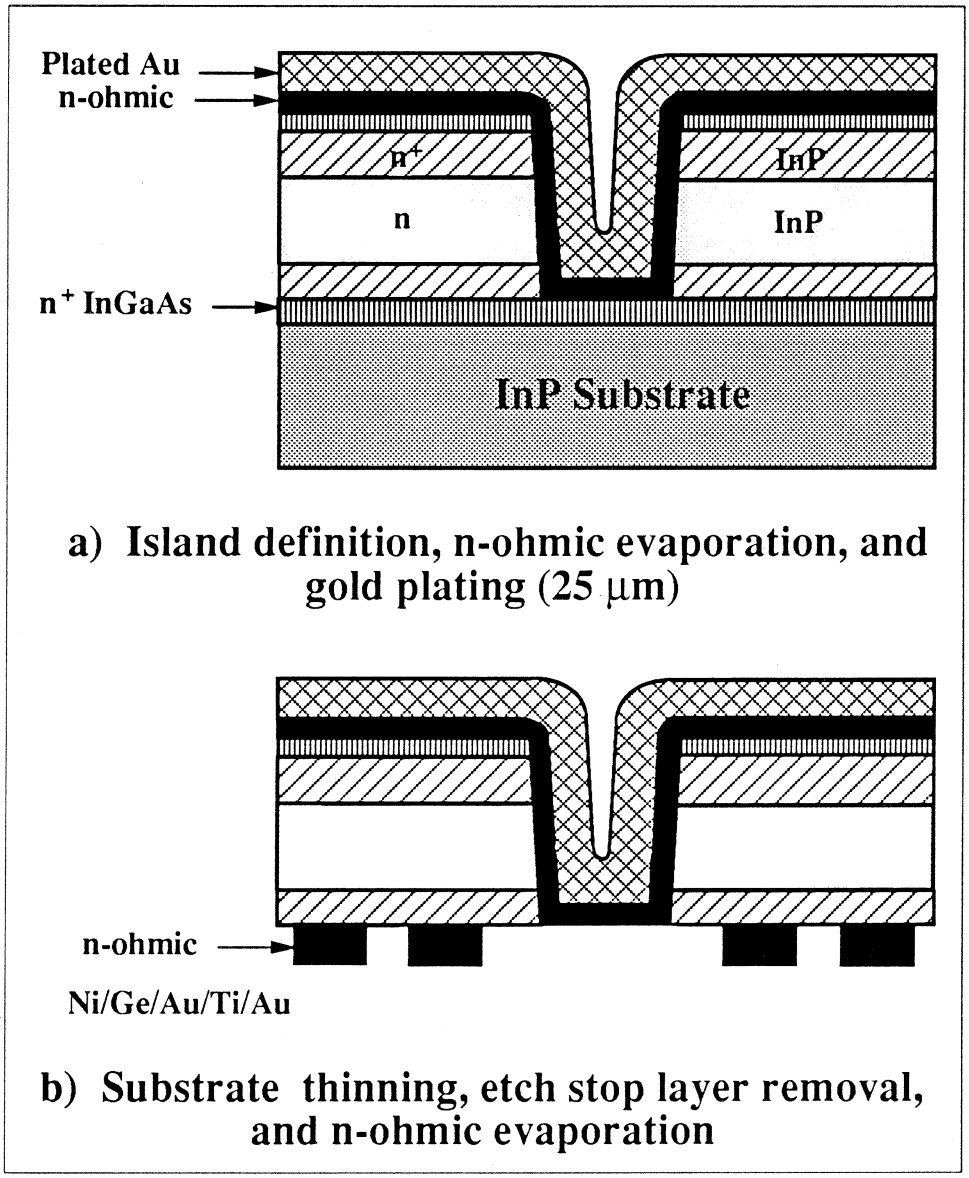

Figure 11: Processing sequence for InP Gunn fabrication

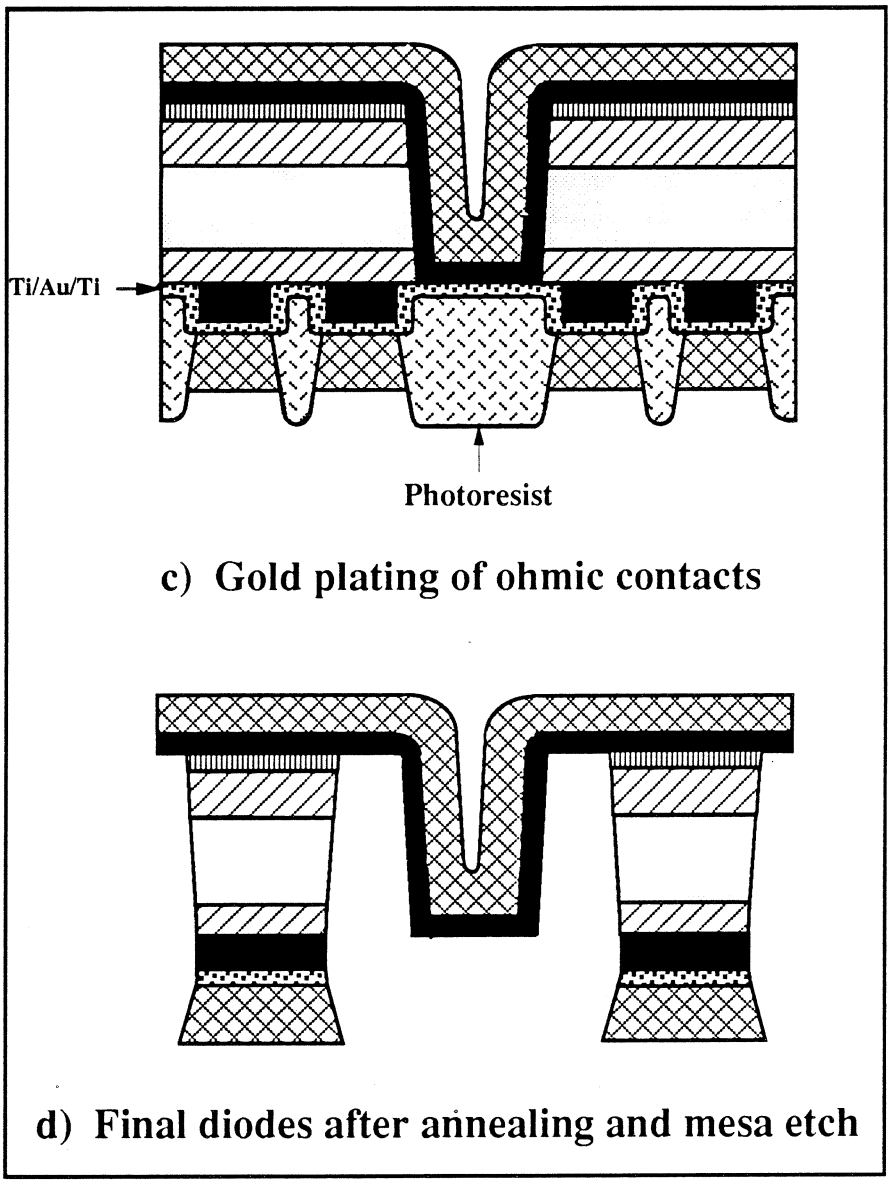

Figure 11: Cont. Processing sequence for InP Gunn fabrication

References

[1] W. Fawcett, A. D. Boardman and S. Swain,"Monte Carlo Determination of Electron Transport Properties in Gallium Arsenide," *J. Phys. Chem. Solids,* **30**, 1969, pp. 643.

[2] K. Brennan, K. Hess, J. Y. Tang, and G. J. Iafrate, "Transient Electronic Transport in InP Under the Condition of High-Energy Electron Injection," *IEEE Trans. on Electron Dev.,* **ED-30**, 12, pp. 1750-1753, Dec. 1983.

[3] D. C. Herbert, W. Fawcett, and C. Hilsum, "High Field Transport in Indium Phosphide," *J. Phys. C: Solid State Phys.,* Vol. 9, pp. 3969-3975, 1976.

[4] G. H. Glover, "Study of Electron energy Relaxation Times in GaAs and InP," *J. Appl. Phys.,* **44**, No. 3, pp. 1295-1301, March 1973.

[5] T. J. Maloney, and J. Frey, "Transient and Steady-State Electron Transport Properties of GaAs and InP," *J. Appl. Phys.,* **48**, No. 2, pp. 781-787, Feb. 1977.

[6] M. V. Fischetti, "Monte Carlo Simulation of Transport in Technologically Significant Semiconductors of the Diamond and Zinc-Blende Structures-Part I: Homogeneous Transport," *IEEE Trans. on Electron Dev.,* **ED-38**, No. 3, pp. 634-649, March 1991.

[7] R. A. Zettler, and A. M. Cowley, "Batch fabrication of Integral-Heat Sink IMPATT Diodes," *Electronics Letters*, Vol. 5, No. 26, pp. 693-694, Dec. 1969.

[8] S. Y. Narayan, J. P. Paczkowski, "Integral Heat Sink Transferred Electron Oscillators," *RCA Review*, Vol. 33, pp. 752-765, Dec. 1972.

[9] A. Paolella, R. L. Ross, and J. Ondria, "Advanced mm-Wave Sources by Automated MBE," *Microwave Journal*, p. 149, April 1986.

[10] J. M. Woodall, J. L. Freeouf, G. D. Pettit, T. Jackson, and P. Kirchner, "Ohmic Contacts to n-GaAs using Graded Band Gap Layers of $Ga_{1-x}In_xAs$ Grown by Molecular Beam Epitaxy," *J. Vac. Sci. Technol.,* **19**, No. 3, Sept./Oct. 1981, p. 626.